Formation of chiral branched nanowires by the Eshelby Twist

JIA ZHU[1], HAILIN PENG[2], A. F. MARSHALL[2], D. M. BARNETT[2], W. D. NIX[2] AND YI CUI[2]*

[1]Department of Electrical Engineering, Stanford University, Stanford, California 94305, USA
[2]Department of Materials Science and Engineering, Stanford University, Stanford, California 94305, USA
*e-mail: yicui@stanford.edu

Published online: 29 June 2008; doi:10.1038/nnano.2008.179

Manipulating the morphology of inorganic nanostructures, such as their chirality and branching structure, has been actively pursued as a means of controlling their electrical, optical and mechanical properties. Notable examples of chiral inorganic nanostructures include carbon nanotubes[1,2], gold multishell nanowires[3], mesoporous nanowires[4,5] and helical nanowires[6–8]. Branched nanostructures[9–16] have also been studied and been shown to have interesting properties for energy harvesting[17] and nanoelectronics[18]. Combining both chiral and branching motifs into nanostructures might provide new materials properties. Here we show a chiral branched PbSe nanowire structure, which is formed by a vapour–liquid–solid branching from a central nanowire with an axial screw dislocation. The chirality is caused by the elastic strain of the axial screw dislocation, which produces a corresponding Eshelby Twist[19,20] in the nanowires. In addition to opening up new opportunities for tailoring the properties of nanomaterials, these chiral branched nanowires also provide a direct visualization of the Eshelby Twist.

Two mechanisms have been widely studied for the growth of micrometre whiskers and, more recently, nanowires (NWs). The first is vapour–liquid–solid (VLS) growth[21], in which metallic particles are typically used as catalysts to promote nucleation and unidirectional growth. The recent development of VLS growth has led to rapid growth in the NW research field[22,23]. Branching can easily be realized by subsequent metal nanoparticle deposition and epitaxial growth on the preformed NWs[10,11,13]. The second mechanism is mediated by an axial screw dislocation[8,24–27]. A screw dislocation that terminates at the surface is known to accommodate atoms efficiently at its step because this is energetically favourable; this also promotes unidirectional growth. The resulting one-dimensional materials have an axial screw dislocation line running along the whiskers.

In 1953, Eshelby[19] conducted a theoretical analysis of a screw dislocation lying parallel to the axis of a thin rod. He showed that the axial screw dislocation induces a torque in a rod of finite length, which in turn leads to an elastic twist of the crystalline lattice and thus the formation of a chiral pattern if at least one end of the rod is free to rotate (Fig. 1a,b). This phenomenon has since been called the Eshelby Twist. It differs from the chirality of other structures, in that it is a result of elastic strain, but without permanent plastic lattice distortion. Despite extensive characterization[8,24–26], there is no direct visualization showing the lattice twisting along the dislocation line. Here we combine VLS and screw dislocation-mediated growths to synthesize NWs with both chiral and branching motifs. The basic concept is shown in Fig. 1. The central NWs are first grown by the screw dislocation-mediated mechanism (Fig. 1a), which produces an Eshelby Twist under the condition that at least one end of NWs is free to rotate (Fig. 1b). Subsequent growth by the VLS mechanism produces branches epitaxially onto the central twisted NWs (Fig. 1c). The arrangement of the pattern of branches provides direct visualization of the Eshelby Twist. We noted similar work by Bierman and colleagues on PbS NWs during the review process of our work[20].

We conducted our study on PbSe branched NW materials[13–16]. The NW synthesis was accomplished in a tube furnace by co-evaporation of low-melting-point metals such as bismuth and PbSe powders at 650 °C for 1–3 h (see Methods). We have previously shown that the low-melting-point metals can be used as a VLS catalyst for the growth of PbSe NWs (ref. 13). In this study, a screw-dislocation-mediated mechanism combined with the VLS mechanism play an important role.

A typical as-grown substrate has two coexisting types of branched NWs with distinct morphology, and each accounts for ~50% of the product, as shown in the scanning electron microscopy (SEM) images of Fig. 2a,b. One type has been studied previously in our group[13] and by others[14–16], and is now called the regular branched NW. These structures occupied about a 10 μm × 10 μm area and have many generations of NW branches (Fig. 2c). All the branches are perpendicular or parallel to each other because PbSe has a rock-salt crystal structure; all the branches grow along the [001] or equivalent growth directions with epitaxial interconnection. The other type occupies a 10 μm × 50 μm elongated area by having NWs branching from a long central NW (Fig. 2e). The immediate branched NWs are perpendicular to the central NW, suggesting the existence of epitaxial conditions with the growth being along the [001] or equivalent directions. Most excitingly, the immediately connected branches rotate around the central NW, forming a chiral pattern (Fig. 2e). This observation suggests that the central NW has its crystalline lattice twisted along its axis, reminiscent of the Eshelby Twist. We term the second type of branched NWs 'chiral branched NWs', which are the focus of this study. There is an additional interesting feature in chiral branched NWs. The length of the central NW is much longer than its branches and those in regular branched NWs; this might be because a screw dislocation with a permanent active growth

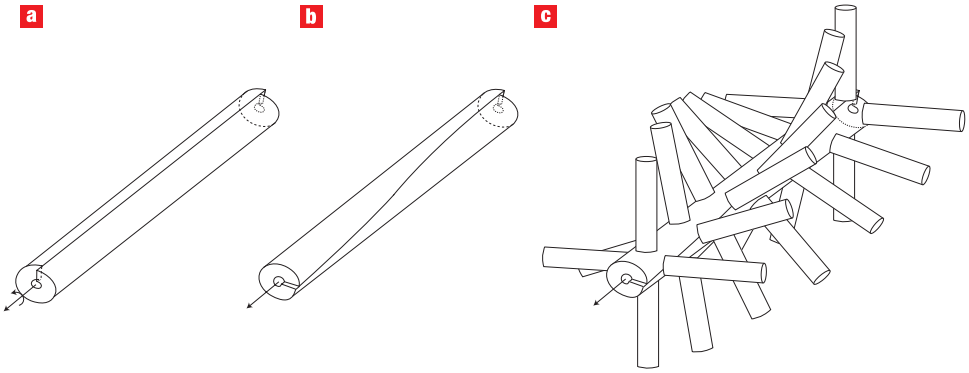

Figure 1 Schematic showing the formation of chiral branched nanowires. a, A NW with an axial screw dislocation in the centre. Both ends of the NW are clamped. **b**, At least one end of the NWs is free to rotate, resulting in an Eshelby Twist. **c**, The branches are grown epitaxially onto the central NW with an axial screw dislocation by VLS growth.

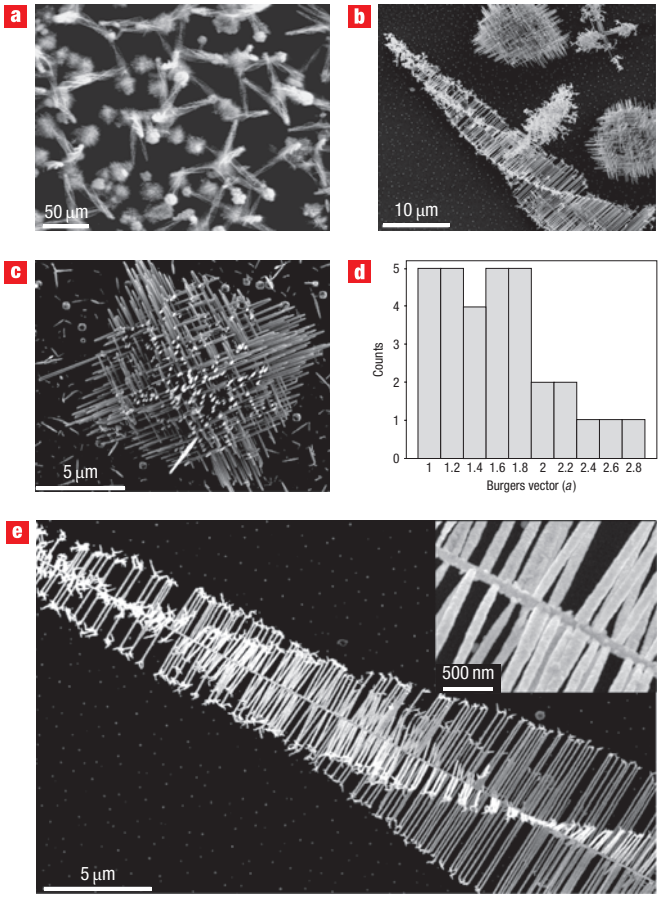

Figure 2 Characterization of regular and chiral branched nanowires. a,**b**, Scanning electron micrographs showing the coexistence of regular and chiral branched PbSe nanowires. **c**, A regular branched NW. **d**, Histogram of the magnitude of the Burgers vector in 31 chiral branched NWs with unit of PbSe lattice constant ($a = 0.612$ nm), assuming round cross-section. **e**, Single chiral branched NWs (inset, high-resolution SEM).

step to incorporate atoms can promote growth much faster than VLS growth. In addition, the low-melting-point catalysts at the tip of branches can be vaporized, which terminates the VLS growth and limits the length of the branches. We have not observed any catalyst particles at the tip of branches[13]. So far, why a screw dislocation is formed within a central NW is not known, although this might be due to nucleation at defects in the substrate or during PbSe island coalescence on the substrate[28].

For a screw dislocation in a thin rod of circular cross-section the twist per unit length has been calculated previously by Eshelby[19] to be $\alpha = -b/(\pi R^2)$, where b is the magnitude of the Burgers vector and R is the rod radius. The length along the rod over which the lattice is twisted by 360° (2π radians) can be calculated to be $L = 2\pi^2(R^2/b)$. Because the rotation of the epitaxial branch directions reflects the twisting of the crystalline lattice in the central NWs, L corresponding to branch rotation by 360° can be directly observed and measured. The radius R can also be measured directly from the high-resolution SEM images (Fig. 2e, inset). Therefore, the expected b can be determined and compared with the lattice constant of PbSe ($a = 0.612$ nm), which can provide evidence for the Eshelby Twist. Figure 2d plots the histogram of results measured over 31 chiral branched NWs. The magnitude of the Burgers vector b is found to be 1–3 times the lattice constant. Bierman and colleagues observed that the Burgers vector in their PbS chiral branched structures has a distribution that is centred around one lattice constant, although it also extends out to several times the lattice constant[20]. In principle b should be an integer multiple of the lattice constant because dislocations with multiple unit Burgers vectors might exist at the centre of the NW. The deviation from an integer in our results might be due to several sources of errors. First, the assumption of a circular cross-section might be erroneous. The central NWs have been found to have round, square or other shaped cross-sections. Second, the surface roughness of central NWs causes a diameter variation along the axis of the NWs. Third, NWs have also been found to be coated with amorphous SiO_x after they are formed. SiO_x is believed to arise the silicon substrate during growth, leading also to an error in determining R. Because b scales with R^2, a small variation in R can cause an appreciable change in b. We estimate that the error in b due to the determination of R can be up to 30%. Fourth, the epitaxial branches can affect how the screw dislocation strain is distributed in central NWs, which would further modify the exact formula for the Eshelby Twist.

To confirm the existence of an axial screw dislocation in the central NW, we have carried out transmission electron microscopy (TEM) studies. The NWs were mechanically transferred to a lacey carbon support film on a TEM copper grid.

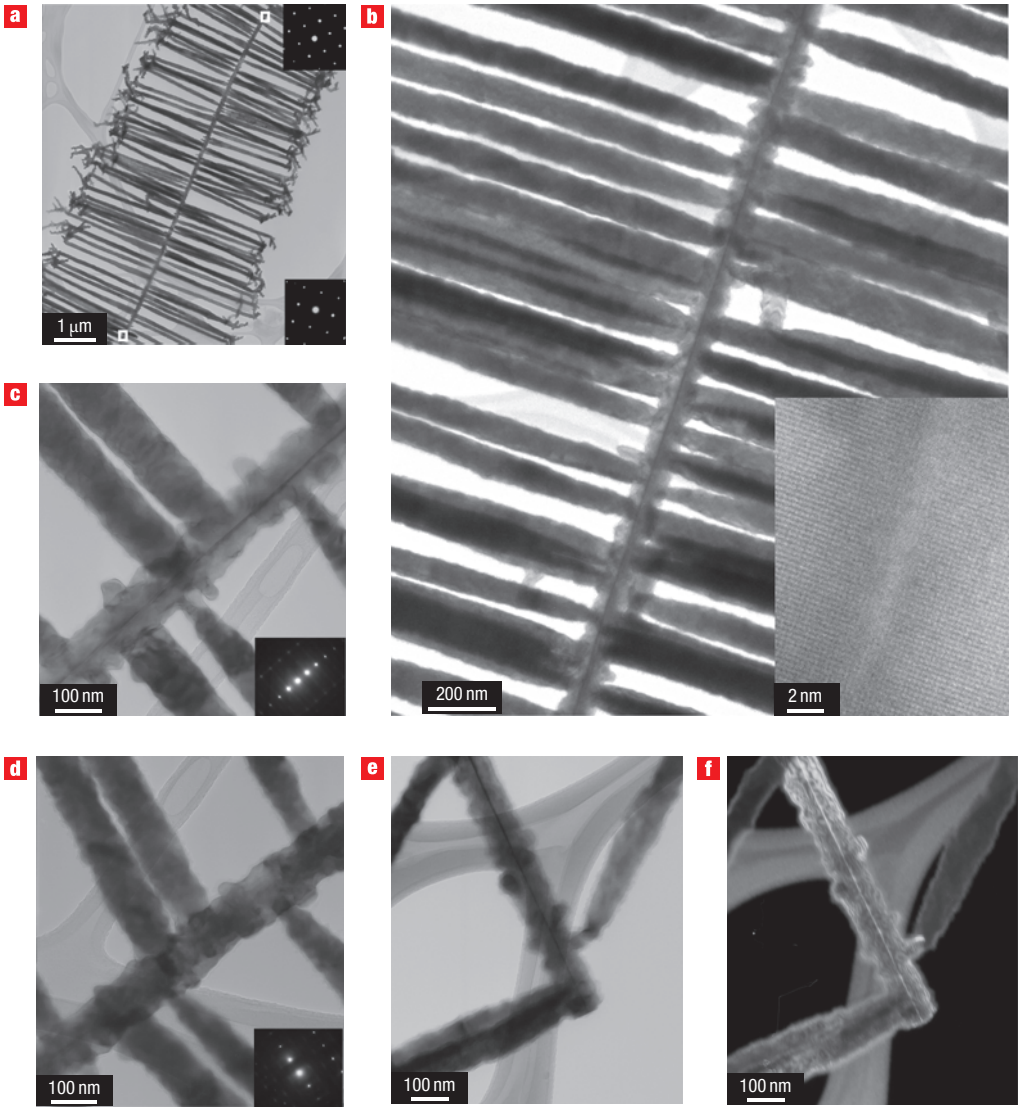

Figure 3 TEM characterization of PbSe chiral branched NWs. a, A single chiral branched NW. The white boxes indicate the positions at which the central NW has twisted 45°. Upper inset: convergent beam electron diffraction (CBED) pattern with a small condenser aperture obtained at the upper box with zone axis along the [110] direction. Lower inset: CBED pattern obtained at the bottom box with zone axis along [100] direction. **b**, Enlarged image of single chiral branched NW with continuous screw dislocation line (black) in the central NW. Inset: high-resolution TEM of a screw dislocation line. **c**, An image of a segment of chiral branched NW taken with the **g** vector of [002] as indicated in the CBED pattern (inset). The dislocation line is clearly identified (black). **d**, An image of the same segment of chiral branched NW as in **c** taken with the **g** vector of [220] as indicated in the inset. The dislocation line disappears in the image. **e**,**f**, Bright-field image (**e**) and dark-field images (**f**) of a segment of chiral branched NW with a continuous screw dislocation line in the central NW.

Figure 3a,b presents bright-field TEM images of chiral branched NWs at lower and higher magnifications, respectively. The dislocation is visible as a continuous dark line that extends from one end of the NW to the other. The central position of the dark line does not change with rotation, confirming a line defect located at the NW centre. High-resolution lattice images such as in the inset in Fig. 3b show that the lattice is free of defects except for the central line defect.

The expected Burgers vector direction for such a propagating screw dislocation in the rock-salt structure is [001], where [001] is also the crystallographic direction of the NW axis. Two-beam imaging confirmed the direction of the Burgers vector as [001], based on the dislocation invisibility criterion, $\mathbf{g} \cdot \mathbf{b} = 0$. Here $\mathbf{b}$ is the Burgers vector and $\mathbf{g}$ is the diffraction vector for a given two-beam condition, the latter referring to a specimen tilt where only one set of planes is at the Bragg diffracting condition, and either the direct or diffracted beam is used to form the image. For our chiral branched NWs, the dislocation was found to be invisible for all diffraction vectors perpendicular to the [001] direction, for example, [200], [020] and [220], whereas it is visible for all other reflections, for example, [111] and [002]. An example is shown in Fig. 3c,d. The image of the screw dislocation line is clearly visible when $\mathbf{g} = [002]$ (Fig. 3c), but disappears when $\mathbf{g} = [220]$ (Fig. 3d). We note that the Burgers vector identified by Bierman and colleagues for their PbS chiral branched NW structures is

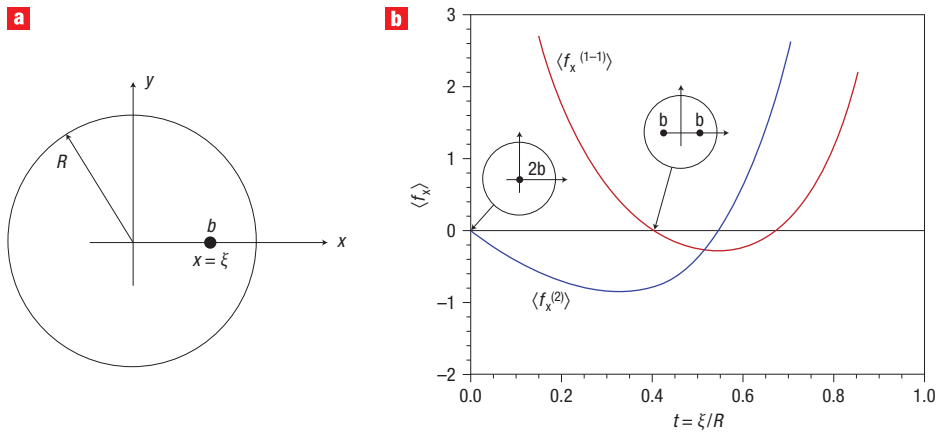

Figure 4 Dislocation force curve simulation. a, Cross section of a NW with a radius of R and screw dislocation line a distance ξ away from the centre. **b**, The force as a function of the normalized distance from the centre of a NW. Two cases are indicated: $\langle f_x^{(2)} \rangle$ for single screw dislocation with a Burgers vector 2**b**, and $\langle f_x^{(1-1)} \rangle$ for two screw dislocation lines each with Burgers vector **b**. The stable state of the axial dislocation line in each case is indicated by an arrow and a cross-sectional view.

different; it is along the [110] direction, although the dislocation line is seen along the [100] long axis of the NWs[20].

In TEM, the electron diffraction is a sensitive way to measure the orientation of the crystalline lattice. We analysed the rotation of the NWs and the period of the chirality using convergent beam electron diffraction (CBED) with a small condenser aperture. This allowed us to follow the rotation by observing the diffraction pattern as we moved the electron probe along the wire axis. For example, starting with the end of the NW oriented at [100] (bottom of Fig. 3a), we observed the diffraction pattern to rotate continuously about the [001] direction as the probe moved along the wire, reaching the [110] orientation (top of Fig. 3a) at a length of $\sim$9.1 μm along the NW axis, which is a 45° rotation of the crystal lattice. Because we are always near the [002] diffracting condition during this exercise, the dislocation stays visible in the image along the NW length, and, again, is observed to maintain a central position. The NW has a diameter of 96 nm, which, assuming a circular cross-section, leads to a calculated value of $b = 0.624$ nm. This magnitude of the Burgers vector is equivalent to one lattice constant of PbSe. Figure 3e, f shows a bright-field and corresponding [002] weak-beam dark-field image on the same segment of a chiral branched NW, where the dislocation is imaged as a narrow white line on a dark background. Weak-beam dark-field imaging can be used to resolve closely spaced dislocations, and such images were observed along the length of several NWs, confirming that only one dislocation line was present in the NWs.

Our experimental results have shown that the axial screw dislocation has the following characteristics: (1) there is only one screw dislocation line, which runs along the centre of the NW; (2) the magnitude of the Burgers vector can be one, two or three times the lattice constant for the NW diameters of 50–200 nm; (3) there is no screw dislocation observed in the side-branched NWs. Eshelby[19] was the first to show, for a rod with a circular cross-section and torque-free end, that such a screw dislocation would find an equilibrium position along the axis of the rod, regardless of the diameter of the rod. This means, perhaps counter-intuitively, that such screw dislocations would also be stable in NWs of arbitrarily small diameters. He also showed that the elastic field of the dislocation would cause the rod to be uniformly twisted; indeed the torsional elastic field associated with the twist provides the stabilizing force causing the dislocation to remain at the centre of the NW. To understand the stability of such a dislocation configuration it is useful to work with the elastic field of a single screw dislocation with a Burgers vector of magnitude b that lies parallel to the z-axis of a rod of radius R, but displaced from the centreline by distance ξ along the x-axis (Fig. 4a). The rod is assumed to be elastically isotropic with shear modulus μ.

If the end of the rod is free to rotate as in our NW case, the image and torsional displacement fields lead to stresses that exert Peach–Koehler forces on the dislocation. After correcting a typographical error in Eshelby[19] and expressing the result in non-dimensional form, we find that the force (per unit length) acting on a single screw dislocation in such a rod is

$$\frac{2\pi R f_x^{(1)}}{\mu b^2} = \langle f_x^{(1)} \rangle = t\left\{\frac{1}{1-t^2} - 2\left(1-t^2\right)\right\} \qquad (1)$$

where $t = \xi/R$. For small t, the force on the dislocation is negative, indicating that the centreline is a stable equilibrium position for the dislocation. If a dislocation with Burgers vector 2**b** is present in the NW then it too would find a stable equilibrium position at the centreline of the wire, provided it does not split into two separate dislocations. The corresponding twist per unit length would be twice that for a single dislocation of Burgers vector **b**, if it is at the centre of the NW. In that case the force on such a super-dislocation would be given by equation (1) with b being replaced by $2b$:

$$\frac{2\pi R f_x^{(2)}}{\mu b^2} = \langle f_x^{(2)} \rangle = 4t\left\{\frac{1}{1-t^2} - 2\left(1-t^2\right)\right\}. \qquad (2)$$

We now consider the case in which a dislocation with Burgers vector 2**b** decomposes into two separate dislocations, each with Burgers vector **b**. These like-signed dislocations would repel each other (say along the x-axis) to reduce the elastic energy of the system. We consider one of the dislocations to be located at $(\xi, 0)$

with the other located at $(-\xi, 0)$. It is easy to express the Peach–Koehler force on the dislocation located at $(\xi, 0)$ as

$$\frac{2\pi R f_x^{(1-1)}}{\mu b^2} = \langle f_x^{(1-1)} \rangle = \frac{1}{2t} + 2t\left\{\frac{t^2}{1-t^4} - 2\left(1-t^2\right)\right\}. \qquad (3)$$

Equations (2) and (3) describe the stability of the super-dislocation or the pair of unit dislocations. These forces are shown as a function of t in Fig. 4b. There we see that $\langle f_x^{(2)} \rangle$ is zero at $t = 0$ and negative for $t < 0.55$. Any super-dislocation within $t < 0.55$ would be expected to glide to the centre of the NW. If the super-dislocation is located in the region $t > 0.55$ then $\langle f_x^{(2)} \rangle$ is positive and the dislocation would glide to the surface of the NW, leaving the NW dislocation free and without an Eshelby Twist. The force acting between the two unit dislocations, $\langle f_x^{(1-1)} \rangle$, is also shown in Fig. 4b. There one sees that the force is positive for $t < 0.4$, indicating that the like-signed dislocations repel each other, as expected. Surprisingly, the force is negative in the domain $0.4 < t < 0.67$ before turning positive again for $t > 0.67$. This means that the two like-signed screw dislocations would find a stable equilibrium configuration at $t \approx 0.4$ (Fig. 4b).

The twist (per unit length) for the pair of dislocations located at $t = \pm 0.4$ is less than that for the super-dislocation at the centre of the NW but greater than that for a single dislocation at the centre of the NW. Although super-dislocations might be expected to separate into single dislocations to reduce the strain energy of the NW, such multiple dislocation lines have not been observed in the PbSe chiral branched NWs. This might be because splitting the super-dislocations into two dislocations requires significant nucleation energy for a new screw dislocation.

METHODS

The synthesis was conducted in a similar way as in our previous studies[13]. A 12-in. horizontal tube furnace (Lindberg/Blue M) equipped with a 1-in.-diameter quartz tube was used. Bismuth powder, as catalyst, was placed in the upstream. The source material, PbSe (Sigma Aldrich, purity 99.999%) was positioned in the middle of the furnace. The substrates, native-oxidized silicon $\langle 100 \rangle$, were placed downstream. A 5% H_2 in N_2 gas mixture acted as a carrier gas to transport vapours from upstream to downstream. The tube was pumped to a base pressure of 60 mTorr and flushed with the carrier gas repeatedly to decrease oxygen contamination. The carrier gas flow rate was maintained at 120 s.c.c.m. at a pressure of 30 Torr during growth. The typical growth temperature was 650 °C, and grow time 1–3 h. The morphology and structure of samples were characterized using an FEI Sirion scanning electron microscope and a Philips CM20 transmission electron microscope operating at 200 kV.

Received 14 March 2008; accepted 5 June 2008; published 29 June 2008.

References

1. Odom, T. W., Huang, J. L., Kim, P. & Lieber, C. M. Atomic structure and electronic properties of single-walled carbon nanotubes. *Nature* **391,** 62–64 (1998).
2. Wildoer, J. W. G., Venema, L. C., Rinzler, A. G., Smalley, R. E. & Dekker, C. Electronic structure of atomically resolved carbon nanotubes. *Nature* **391,** 59–62 (1998).
3. Kondo, Y. & Takayanagi, K. Synthesis and characterization of helical multi-shell gold nanowires. *Science* **289,** 606–608 (2000).
4. Che, S. *et al.* Synthesis and characterization of chiral mesoporous silica. *Nature* **429,** 281–284 (2004).
5. Wu, Y. Y. *et al.* Composite mesostructures by nano-confinement. *Nature Mater.* **3,** 816–822 (2004).
6. Gao, P. X. *et al.* Conversion of zinc oxide nanobelts into superlattice-structured nanohelices. *Science* **309,** 1700–1704 (2005).
7. Meister, S. *et al.* Synthesis and characterization of phase-change nanowires. *Nano Lett.* **6,** 1514–1517 (2006).
8. Zhang, H. F., Wang, C. M. & Wang, L. S. Helical crystalline SiC/SiO_2 core–shell nanowires. *Nano Lett.* **2,** 941–944 (2002).
9. Manna, L., Milliron, D. J., Meisel, A., Scher, E. C. & Alivisatos, A. P. Controlled growth of tetrapod-branched inorganic nanocrystals. *Nature Mater.* **2,** 382–385 (2003).
10. Dick, K. A. *et al.* Synthesis of branched 'nanotrees' by controlled seeding of multiple branching events. *Nature Mater.* **3,** 380–384 (2004).
11. Wang, D., Qian, F., Yang, C., Zhong, Z. H. & Lieber, C. M. Rational growth of branched and hyperbranched nanowire structures. *Nano Lett.* **4,** 871–874 (2004).
12. May, S. J., Zheng, J. G., Wessels, B. W. & Lauhon, L. J. Dendritic nanowire growth mediated by a self-assembled catalyst. *Adv. Mater.* **17,** 598–602 (2005).
13. Zhu, J. *et al.* Hyperbranched lead selenide nanowire networks. *Nano Lett.* **7,** 1095–1099 (2007).
14. Fardy, M., Hochbaum, A. I., Goldberger, J., Zhang, M. M. & Yang, P. D. Synthesis and thermoelectrical characterization of lead chalcogenide nanowires. *Adv. Mater.* **19,** 3047–3051 (2007).
15. Bierman, M. J., Lau, Y. K. A. & Jin, S. Hyperbranched PbS and PbSe nanowires and the effect of hydrogen gas on their synthesis. *Nano Lett.* **7,** 2907–2912 (2007).
16. Ge, J. P. *et al.* Orthogonal PbS nanowire arrays and networks and their Raman scattering behaviour. *Chem. Eur. J.* **11,** 1889–1894 (2005).
17. Sun, B. Q., Marx, E. & Greenham, N. C. Photovoltaic devices using blends of branched CdSe nanoparticles and conjugated polymers. *Nano Lett.* **3,** 961–963 (2003).
18. Cui, Y., Banin, U., Bjork, M. T. & Alivisatos, A. P. Electrical transport through a single nanoscale semiconductor branch point. *Nano Lett.* **5,** 1519–1523 (2004).
19. Eshelby, J. D. Screw dislocations in thin rods. *J. Appl. Phys.* **24,** 176–179 (1953).
20. Bierman, M. J., Lau, Y. H. A., Kvit, A. V., Schmitt, A. L. & Jin, S. Dislocation-driven nanowire growth and Eshelby Twist. *Science* **320,** 1060–1063 (2008).
21. Wagner, R. S. & Ellis, W. C. Vapour–liquid–solid mechanism of single crystal growth. *Appl. Phys. Lett.* **4,** 89–90 (1964).
22. Lieber, C. M. Nanoscale science and technology: Building a big future from small things. *MRS Bull.* **28,** 486–491 (2003).
23. Yang, P. The chemistry and physics of semiconductor nanowires. *MRS Bull.* **30,** 85–91 (2005).
24. Sears, G. W. Twist in lithium fluoride whiskers. *J. Chem. Phys.* **31,** 53–54 (1959).
25. Sears, G. W., DeVries, R. C. & Huffine, C. Twist in alumina whiskers. *J. Chem. Phys.* **34,** 2142–2143 (1961).
26. Veblen, D. R. & Post, J. E. A TEM study of fibrous cuprite (chalcotrichite): microstructures and growth mechanisms. *Am. Mineral.* **68,** 790–803 (1983).
27. Drum, C. M. Twist and axial imperfections in filamentary crystals of aluminum nitride. II. *J. Appl. Phy.* **36,** 824–829 (1965).
28. Gerber, C., Anselmetti, D., Bednorz, J. G., Mannhart, J. & Schlom, D. G. Screw dislocations in high-T_c films. *Nature* **350,** 279–280 (1991).

Acknowledgements

Y.C. acknowledges support from the Stanford Global Energy and Climate Project and the Center for Probing the Nanoscale (CPN) with National Science Foundation (NSF) grant PHY-0425897. J.Z. is a CPN Fellow. W.D.N. acknowledges support by the Office of Science, Office of Basic Energy Sciences, of the US Department of Energy under grant DE-FG02-04ER46163.

Author contributions

J.Z. and Y.C. conceived and designed the experiments. J.Z., A.F.M. and HP. performed the experiments. D.M.B. and W.D.N. performed simulation. J.Z., A.F.M., W.D.N. and Y.C. co-wrote the paper. All authors discussed the results and commented on the manuscript.

Author information

Reprints and permission information is available online at http://npg.nature.com/reprintsandpermissions/. Correspondence and requests for materials should be addressed to Y.C.